THE PENNSYLVANIA STATE UNIVERSITY

ERRORS IN MEASURING THE FLUCTUATING FLOW AT THE DISCHARGE OF AN INDUCER

by

Harry G. McCafferty

DEPARTMENT OF AEROSPACE ENGINEERING

UNIVERSITY PARK, PENNSYLVANIA

The Pennsylvania State University

The Graduate School

Department of Aerospace Engineering

Errors in Measuring the Fluctuating Flow at the Discharge of an Inducer

A Thesis in

Aerospace Engineering

by

Harry G. McCafferty

Submitted in partial fulfillment
of the requirements
for the degree of

Master of Science

June 1967

Approved:

_____

Assistant Professor of Aerospace Engineering, Thesis Adviser

_____

Head of the Department of Aerospace Engineering

ACKNOWLEDGMENT

The author would like to express his gratitude to his thesis adviser, Dr. B. Lakshminarayana, and to the Department Head, Dr. George F. Wislicenus, without whose advice and guidance this thesis would not have been possible.

The research contained in this paper was carried out under the sponsorship of the National Aeronautics and Space Administration, and was conducted at The Pennsylvania State University, and is currently operating under Contract No. NsG 537.

TABLE OF CONTENTS

ABSTRACT

Rotating total and static pressure probes were used to obtain the circumferential variation of the discharge pressure produced by an axial flow inducer. The spacial average values of these pressure measurements were compared with the static and total pressure measurements obtained by stationary pressure probes located at the same axial and radial station as the rotating probes. For the inducer discharge flow field considered in this investigation both the pressure and the direction of the discharge flow were varying and the pressure fluctuations were small compared to the time average values. The inducer discharge velocity triangles derived from the rotating and stationary probe measurements were compared.

It was found that the stationary static pressure probe recorded a pressure larger than the time average value and that the error between the total pressure recorded by the stationary probe and the time average total pressure was small.

Also a theoretical discussion of the various errors and corrections involved in such pressure measurements is presented.

LIST OF FIGURES

NOMENCLATURE

Symbol	Definition
q	Dynamic pressure
p_S	Gage static pressure used for probe calibration curve
p_T	Gage total pressure used for probe calibration curve
P_m	Measured static pressure in turbulent flow
P_{T_m}	Measured total pressure in turbulent flow
$\bar{P}_S$	Time average static pressure in turbulent flow
p'	Gage pressure fluctuation about the time average value
P'_{max}	Amplitude of the manometer input fluctuating pressure
ΔP_W	Pressure differential acting upon wedge probe face
H_R	Gage total pressure of the relative flow
$\psi_{T_{ab}}$	Non-dimensional total pressure of the absolute flow $\left(\frac{2gH_R}{U_t^2}\right)$
h_S	Gage static pressure of the relative flow
ψ_S	Non-dimensional static pressure coefficient $\left(\frac{2gh_s}{U_t^2}\right)$
$\bar{\psi}_{T_{ab}}$	Spacial average of $\psi_{T_{ab}}$ over one blade passage
$\bar{\psi}_S$	Spacial average of ψ_S over one blade passage
u', v', w'	Turbulent velocity components

Symbol	Definition
$\bar{U}$	Time average velocity of flow parallel to probe axis in turbulent flow
U_t	Blade tip velocity
V	Inducer absolute flow discharge velocity
V_θ	Tangential component of the inducer absolute flow discharge velocity
W	Inducer relative flow discharge velocity
W_θ	Tangential component of the inducer relative flow discharge velocity
r	Radial location of the pressure probe
R	Radius of the tubing containing the manometer fluid
R_o	Radius of the cylindrical manometer reservoir
L	Total length of the manometer fluid corresponding to the time average pressure
x'	Manometer fluid level fluctuation about the time average value
x'_p	Particular solution to the differential equation
x'_c	Complementary solution to the differential equation
λ	Flow angle of attack with respect to the probe axis
α	Inducer absolute discharge flow angle with respect to the tangential direction
β	Inducer relative discharge flow angle with respect to the tangential direction
δ	Probe displacement distance in shear flow
θ	Phase angle
ω	Frequency of the manometer input pressure fluctuation in radians per second

Symbol	Definition
ρ	Fluid density
μ	Fluid dynamic viscosity
γ	Fluid specific weight
τ	Wall shear stress for the manometer tubing

Subscripts

$\lambda = 0$	Probe aligned in flow direction
S	Static pressure
T	Total pressure
ab	Absolute flow
t	Inducer blade tip

Superscripts

$\cdot$	Derivative with respect to time
$-$	Time average value

I. INTRODUCTION

Statement of the Problem

Conventional pressure probes have often been used to survey the fluctuating flow field behind rotating blade rows in turbomachinery. An attempt has been made in this thesis to investigate both analytically and experimentally the errors involved in such pressure measurements under conditions where the blade boundary layers extend over a major portion if not the entire cross section between the blades. It is not known what a stationary probe connected to a manometer would read under these conditions. The purpose of this study is to estimate and measure the difference between the time average of the input pressure variation, obtained by a rotating probe system, and the pressure obtained by a stationary probe.

Both the static and stagnation pressure variation in the circumferential direction were obtained by means of a rotating probe system. The spacial average across one blade passage was then compared and correlated with the results obtained from stationary static and total pressure probes located at the same station.

Origin and Importance of the Study

Basic fluid mechanic research on a model inducer, used to increase the suction specific speed of centrifugal impellers for missiles and rocket engines, is being conducted at this University. It is known that inducers, like most turbomachinery, produce a fluctuating pressure and that the direction of the discharge flow varies across the blade passage. The origin of this study was the desire to interpret the

meaning of the pressure measurements obtained with a stationary probe behind the rotating inducer blade row and to determine the relative velocity distribution between the blades at the inducer discharge. A description of the inducer and the static and total pressure probe employed in this investigation is given in the Figures 1 - 8.

The interpretation of pressure measurements carried out in a flow field which has a fluctuating pressure and varying flow direction is known to be important in turbomachinery research. Other examples where probes are exposed to fluctuating pressure deal with obtaining the inlet and exhaust pressure for reciprocating engines and in measuring the pressure in a variety of pipe line situations encountered in industrial applications.

Previous Related Studies

A careful inspection of the existing literature has revealed that a considerable amount of work has been directed towards the errors associated with pressure measurements in a fluctuating flow field. The procedure followed in most of the past investigations has been to isolate and study a particular source of error.

The discharge flow field for most turbomachinery is one area where several error producing effects simultaneously exist. Literature dealing with the combined effect of the various error producing effects is meager, particularly under conditions where the total head varies across the entire blade passage.

In the theoretical discussion of this thesis, the various error producing effects have been described and a critical presentation of

the pertinent existing literature has been given. The necessary modifications of the previous work and the development of new material has also been included in order to complete the theoretical discussion for the particular model being considered.

II. THEORETICAL DISCUSSION

Introduction and Discussion

In this chapter attempts are made to describe and predict the various error producing effects associated with static and total pressure measurements obtained from both rotating and stationary pressure probes. Methods of applying the results from previous studies to this particular investigation are also given. The five error producing effects considered in the investigation are as follows: (1) variation in flow direction, (2) turbulence, (3) shear flow effects, (4) alteration of the pressure waves which propagate through the connecting tubing, and (5) manometer response to a fluctuating pressure.

Errors in Stationary Probe Pressure Measurements

Error Due to Variations in Flow Direction

In the absence of secondary flow and directional change due to turbulence, any deviation in the discharge flow direction from that of the main stream direction occurs inside the blade wake. As seen by a stationary probe, both the pressure and direction of the oncoming flow are varying. When a static or total pressure probe is placed in this directionally varying flow, the measurements may be in error. This is particularly true for the inducer since long blade passages and the associated fluid frictional effects produce a blade wake which is a major portion of the discharge flow field.

In practice the usual procedure is to align the probe in the discharge direction of the absolute main flow. As the wake sweeps

past the probe, the flow in the wake is at an angle of attack (λ) with respect to the probe axis. The extent to which the flow angle varies inside the wake dictates the probe error.

The static pressure probe must be aligned in the direction of the flow (with the static holes normal to the flow direction) in order to record the true static pressure. When the axis of the probe is at an angle of attack (λ) to the flow direction, the probe picks up a part of the dynamic component of the pressure in addition to the true static pressure. The difference between the probe reading and the true static pressure arises from the impact of the transverse component of velocity on the probe and its holes. The probe error depends upon the design of the probe, especially on the number, size and arrangement of the static holes, and on the magnitude and frequency of the cross component of velocity. A calibration curve

$$\left[\frac{p_s - p_{\lambda=0}}{q} \text{ v. s. } \lambda \right]$$

for the particular probe is a simple method for obtaining an estimate of the static pressure probe error if the maximum flow deviation is known.

For the total pressure probe, if the maximum angle of attack (λ) of the oncoming flow is less than the specified probe sensitivity angle, then the effect of the varying flow may be neglected. The sensitivity angle is defined as the angle of attack at which the total pressure error reaches a value of one per cent of the true total pressure. For angles of attack greater than the sensitivity angle, it is necessary again to construct a calibration curve

$$\left[\frac{P_T - P_{T_{\lambda=0}}}{q} \quad \text{v.s.} \quad \lambda \right]$$

for the particular probe in order to obtain an estimate of the total pressure probe error if the maximum flow deviation is known.

For a known pressure gradient and ideal, potential velocity distribution, the Truckenbrolt (1) method can be used to calculate the turbulent boundary layer profile along the blade. The mean flow angles inside the wake at the blade trailing edge can be obtained graphically. For a given distance downstream of the trailing edge, the flow angles inside the wake can be obtained using the analysis presented by Lakshminarayana and Horlock (2).

Error Due to Turbulence

In turbulent flow the conventional static pressure probe registers a larger reading than the true average static pressure. This error is due to the impact pressure of the transverse fluctuating components of the turbulent velocity. For a static pressure probe, aligned in the direction of the mean flow, Goldstein (3) gives the relationship between the measured pressure (P_m) and the time average static pressure ($\overline{P}_s$) as follows:

$$P_m = \overline{P}_s + K_s \rho \left(\overline{v'^2} + \overline{w'^2} \right) \qquad (1)$$

where v' and w' are the turbulent fluctuating velocity components and k_s is a numerical factor which has a characteristic value for

the particular static pressure probes in turbulent flow. Fage (4) has conducted a series of experiments in order to obtain a numerical value for k_s. The results obtained from Fage's experiments indicate that $k_s = 0.25$ for fully developed turbulent flow. In the case of fully developed turbulent flow, the expression for the measurements obtained from a static pressure probe and the true average static pressure can be written as follows:

$$P_m = P_s + \tfrac{1}{4} \rho \left(\overline{v'^2} + \overline{w'^2} \right) \tag{2}$$

For isotropic turbulent flow $\overline{v'^2} = \overline{w'^2}$ and the measured pressure exceeds the true pressure by $\frac{1}{2} \rho \overline{v'^2}$.

A rotating wedge probe was used to determine the circumferential static pressure distribution across one of the four blade passages. The influence of turbulence upon the measured pressure (P_m) is shown as follows:

$$P_m = P_s + K_s \rho \left(\overline{v'^2} \right) \tag{3}$$

where v' is the turbulent velocity component normal to the wedge face and k_s is a numerical factor which must be determined experimentally for the particular wedge probe.

In a theoretical study, Goldstein found that the total pressure probe measures the stagnation pressure of the total velocity vector. His analysis was based on the assumption that the frontal part of the probe might be considered as a stagnation point. A total pressure

probe aligned in the direction of the mean flow would read as the following:

$$P_{T_m} = \overline{P}_s + \tfrac{1}{2}\rho\left[\overline{(U+u')^2} + \overline{v'^2} + \overline{w'^2}\right] \qquad (4)$$

where $\overline{U}$ is the mean velocity of the flow parallel to the probe axis and u', v' and w' are the turbulent velocity components. For isotropic turbulent flow $\overline{u'^2} = \overline{v'^2} = \overline{w'^2}$ and the pressure reading would be as follows:

$$P_{T_m} = \overline{P}_s + \tfrac{1}{2}\rho\left[\overline{U}^2 + \overline{3u'^2}\right] \qquad (5)$$

The hot-wire anemometer may be used to determine the turbulent velocity components.

The problem of measuring the turbulence level in turbomachinery becomes even more complex since the discharge flow is composed of a periodic fluctuating velocity due to the blade wake in addition to aperiodic turbulence component. In order to determine the turbulence level, it becomes necessary to use a rotating hot-wire inside the blade passage and carry out a traverse across the blade passage to obtain the variation of the turbulence intensity across the passage.

Error Due to the Influence of the Connecting Tubing

The alteration of the pressure waves which propagate through the connecting tubing between the pressure probe and the manometer is due to the following: (1) variation in propagation velocity with

fluctuating pressure; (2) wave attenuation due to viscosity and wall friction; and (3) wave reflection at both ends of the connecting tubing. For the inducer considered in this investigation the discharge pressure fluctuations were small compared to the time average pressures (maximum $\frac{\Delta P}{\bar{P}} = 0.0002$) and the effects of the connecting tubing mentioned above were neglected.

Manometer Response

The dynamic response of a manometer to an input pressure which varies with time will be considered next. In the manometer tube the inertia and viscosity of air may be considered negligible compared with the manometer liquid. If the manometer liquid is considered as a free body the primary forces which act upon it are as follows:

(1) The gravity force (weight) of the manometer liquid.

(2) The friction force at the interface between the liquid and the wall of the tube.

(3) The pressure differential acting upon the two ends of the manometer liquid.

(4) The acceleration force of the fluctuating manometer liquid.

One leg of the micromanometer used in this investigation contained a fluid reservoir which was exposed to the fluctuating pressure. The other leg was a tube of small diameter and was exposed to the atmosphere. The displacement of the fluctuating manometer fluid was measured in this tube. Therefore, any small pressure differential would affect the liquid height in the tube and any change in the reservoir height was negligibly small. With this in mind, the gravity force and the fluid friction due to the fluctuating column of the manometer liquid can be considered negligible for the manometer reservoir fluid.

For laminar liquid flow in the manometer tubing, the wall shearing stress (τ) can be expressed in terms of the average velocity ($\dot{x}'$) across the pipe section as follows:

$$\tau = \frac{4\mu\dot{x}'}{R} \tag{6}$$

where R is the radius of the tubing containing the manometer fluid.

Based on the kinetic energy of steady laminar flow, the effective mass of the moving liquid is considered to be four-thirds of its actual mass. Applying Newton's second law to the manometer as a free body, the vertical height of the fluid fluctuation x' about the displacement corresponding to the time average of the input pressure, can be expressed as follows:

$$\pi R_o^2 p(t)' - \pi R^2 \gamma x' - 2\pi R L \frac{4\mu\dot{x}'}{R} = \frac{4}{3}\frac{\pi R^2 L \gamma}{g}\ddot{x}' \tag{7}$$

where p(t)' is the pressure fluctuation about the time average input pressure acting on the fluid inside the reservoir, R_o is the radius of the cylindrical reservoir, R is the radius of the tubing containing the manometer fluid, γ is the fluid specific weight of the manometer fluid, μ is the viscosity of the manometer fluid, and L is the total length of the fluid column corresponding to the time average pressure. The four terms in the above expression correspond to the pressure force, gravity force, friction force and inertia force, respectively. Upon rearranging, the above expression takes on the form as follows:

$$\ddot{x}' + \frac{6\mu g}{\gamma R^2}\dot{x}' + \frac{3g}{4L}x' = \frac{3g}{4L\gamma}\left(\frac{R_o}{R}\right)^2 p'(t) \qquad (8)$$

A similar second order linear differential equation was derived by Doebeline (5) for a simple U - tube configuration.

The general solution to the above second order linear differential equation is composed of a complementary solution plus a particular solution. The exact form of the complementary solution depends upon the nature of the roots of the quadratic equation obtained by writing the differential equation in operator form. The roots of the quadratic equation are as follows:

$$\Sigma = \frac{-3\mu g}{\gamma R} - \sqrt{\left(\frac{3\mu g}{\gamma R}\right)^2 - \frac{3g}{4L}} \qquad (9)$$

$$\phi = \frac{-3\mu g}{\gamma R} + \sqrt{\left(\frac{3\mu g}{\gamma R}\right)^2 - \frac{3g}{4L}} \qquad (10)$$

For the case of supercritical damping, $\left(\frac{3\mu g}{\gamma R}\right)^2 > \frac{3g}{4L}$

and both Σ and ϕ are real and negative and the general form of the complementary solution is as follows:

$$x_c' = c_1 e^{\Sigma t} + c_2 e^{\phi t} \qquad (11)$$

where c_1 and c_2 are constants and depend upon the initial conditions.

Both exponential terms are negative and vanish as time t becomes large and as a result the complementary solution vanishes for the case of supercritical damping.

For the case of critical damping, $\left(\frac{3\mu g}{\gamma R}\right)^2 = \frac{3g}{4L}$ and the solution of the quadratic equation is single valued and is equal to $-\frac{3\mu g}{\gamma R}$. The general form of the complementary solution is as follows: $X_c' = e^{\Sigma t}\left[c_1 + c_2 t\right]$ where $\Sigma = -\frac{3\mu g}{\gamma R}$, and c_1 and c_2 are constants and depend upon the initial conditions. For increasing time (t), $e^{\Sigma t}$ approaches zero faster than $c_2 t$ approaches infinity and the complementary solution for the case of critical damping vanishes.

For the case of subcritical damping, $\left(\frac{3\mu g}{\gamma R}\right)^2 < \frac{3g}{4L}$ and both Σ and Φ are complete roots with negative real parts. After some rearranging the general form of the complementary solution is as follows:

$$X_c' = c_1 e^{-\zeta K t} \sin(bt + \theta) \qquad (12)$$

where ζ is the ratio of the manometer fluid viscosity to that viscosity which the fluid must have for critical damping, $K = \sqrt{\frac{3g}{4L}}$, and b represents the damped circular frequency and is equal to $\sqrt{\left(\frac{3g}{4L}\right)\left(1-\zeta\right)^2}$. c_1 and θ are constants and must be determined by initial conditions. The first part, $c_1 e^{-\zeta K t}$, represents a decaying amplitude for the trigonometric function $\sin(b t + \theta)$. Thus, the motion is oscillatory but with an amplitude which reduces with time. The above analysis has shown that the three possible com-

plementary solutions are transient and in time will vanish. The solution of the differential equation for the manometer fluctuation is essentially the particular solution and will be discussed next.

In order to determine the general form of the particular solution to the second order linear differential equation which governs the manometer fluctuation, the nature of the fluctuating input pressure to the manometer must be known. Generally speaking this input function must be determined experimentally since in practice the pressure fluctuation to which the pressure probe is exposed is usually not known. The influence of the connecting tubing is quite complicated and presently its influence upon the pressure waves are not completely understood. For these reasons the input pressure fluctuation to the manometer must be obtained by experimentally determining the pressure fluctuation at the end of the connecting tubing. The piezoelectric transducer* has a very high natural frequency and little damping and should be adequate for obtaining the form of the pressure fluctuation at the end of the connecting tubing.

For the inducer test model considered in this investigation the total pressure fluctuation was the largest for the blade tip section. The total pressure variation is shown in Figure 9 and should have the greatest influence upon the manometer response. In order to obtain an estimation of the manometer response to this pressure fluctuation the pressure variation may be represented by a sine wave. It, therefore, becomes meaningful to investigate the particular solution of

---

* An attempt to do this was unsuccessful since the output pressure differential was very small (one millivolt) in the case of the inducer and the instrument noise prevented meaningful measurements of the pressure wave form.

the differential equation when the input pressure acting on the fluid inside the reservoir is of the form $P'_{max} \sin \omega t$.

The particular solution can be written in the following form:

$$X'_p = A \sin \omega t + B \cos \omega t \tag{13}$$

Trigonometric substitutions enable the above solution to be written in the following form:

$$X'_p = \sqrt{A^2 + B^2} \sin (\omega t - \theta) \tag{14}$$

where $$\text{TAN } \theta = -\frac{B}{A}$$

The constant coefficients A and B are determined by substituting the first expression for the particular solution into the differential equation and then equating the coefficients of the sine terms and similarly equating those for the cosine terms. Having determined A and B the expression for the particular solution becomes:

$$X'_p = \frac{P'_{max}\left(\frac{R_o}{R}\right)^2 \sin(\omega t - \theta)}{\sqrt{\gamma^2\left(1 - \frac{4L\omega^2}{3g}\right)^2 + \left(\frac{8\mu L\omega}{R^2}\right)^2}} \tag{15}$$

$$\text{TAN } \theta = \frac{8\mu L\omega}{R^2\gamma\left(1 - \frac{4L}{3g}\omega^2\right)}$$

Where P'_{max} is the amplitude of the manometer input fluctuating pressure.

The above particular solution represents the steady state motion of the manometer liquid. This motion has the same frequency as the fluctuating input pressure and lags behind the input function by the phase angle θ. For a given manometer, manometer fluid, and input amplitude, the amplitude of the steady state motion depends upon the frequency ω of the fluctuating input pressure and the length (L) of the fluid column corresponding to the time average pressure. When the time average input pressure is large compared to the amplitude of the fluctuation about the average, the total length (L) of the fluid column corresponding to the time average pressure along with the square of the frequency of the pressure fluctuation can produce a large value of $\frac{4L}{3g}\omega^2$. For $\frac{4L}{3g}\omega^2 \gg 1$, the particular solution to the differential equation approaches zero. As a result, the fluctuation in the manometer reading becomes small. The behavior of the manometer used in this investigation is discussed in the section dealing with discussion and conclusions.

Correction and Errors for Rotating Probe Pressure Measurements

In order to obtain the true static and total pressure distribution across one of the four blade passages obtained from a rotating pressure probe, the pressure measurements had to be corrected for the centrifugal force effect. The sources of possible errors for the rotating pressure probe measurements to be considered are the effects of shear flow.

Centrifugal Force Correction

The centrifugal force correction for both the static and total

pressure measurements can be obtained by applying the condition of radial equilibrium to a rotating column of air. For the incompressible flow model, the following relationship between the pressure recorded from a rotating probe and the true local absolute pressure is as follows:

$$P_L - P_r = \tfrac{1}{2} \rho \Omega^2 \left(r_p^2 - r_d^2 \right) \tag{16}$$

where

p_L = the true local absolute pressure

p_r = the uncorrected absolute pressure recorded by the manometer

r_p = the radius to the probe inlet

r_d = the radius to the orifice in the rotating pressure transfer device

Ω = angular velocity of the rotating probes

Error Due to Shear Flow

The inducer blade wake shear flow is a possible source of error for both the pressure and flow direction measurements. The shear flow effect on the wedge probe used for measuring the circumferential variation of the inducer discharge relative flow direction is considered first. The wedge probe was calibrated by plotting the pressure differential acting upon the wedge faces divided by the dynamic pressure of the flow against the angle which the probe made with the oncoming flow $\left[\frac{\Delta P_w}{q} \text{ v.s. } \lambda \right]$. The calibration of the wedge probe was conducted in a wind tunnel where the flow was uniform. The shear flow error

arises because the inducer discharge flow field is non-uniform in the circumferential direction. For any measured pressure differential acting upon the faces of the wedge probe, the flow angle obtained from the calibration curve is different from the true discharge flow direction for any given radial and circumferential position. The extent to which the wake shear flow produces an error in flow direction measurements depends upon the relative flow total pressure gradient and the distance between the pressure taps on the wedge probe faces.

The second source of error due to the shear flow in the inducer blade wake involves the displacement of the relative flow total pressure profile from its true position. This is due to the circumferential total pressure gradient at the total pressure probe inlet. In a uniform flow field, the effective center of pressure lies on the probe axis. But in shear flow the effective center of pressure is displaced from the probe axis towards the region of higher velocity. For the inducer considered in this investigation the error due to the displacement of the total pressure profile is negligible because a maximum displacement of one half the probe diameter is small compared to the wake width and the shear gradient is small.

In cases where the probe displacement might be important, Lighthill (6) has developed a theoretical expression in order to correct the measured velocity profile assuming that the static pressure is constant. Lighthill's expression for the displacement (δ) of the effective center of pressure from the probe axis is in terms of the velocity (W) along the axis of the Pitot tube, the outside

diameter (D) of the cylindrical probe and the shear derivative ($\frac{\partial W}{\partial Y}$). From dimensional considerations the non-dimensional functional displacement correction ($\frac{\delta}{D}$) can be written as follows:

$$\frac{\delta}{D} = \text{Function} \left[\frac{\left(\frac{\partial W}{\partial Y}\right) D}{2 U} \right] \tag{17}$$

Lighthill's analysis for the displacement of the stagnation streamline from its position at infinity also considers the "downwash" (secondary flow component perpendicular to the undisturbed flow) on the dividing streamline. His final expression for the displacement effect is as follows:

$$\frac{\delta}{D} = 0.45 \left[\frac{\left(\frac{\partial W}{\partial Y}\right) D}{2 W} \right] - 3.05 \left[\frac{\left(\frac{\partial W}{\partial Y}\right) D}{2 W} \right]^3 \tag{18}$$

As mentioned previously, the error due to the displacement of the total pressure profile for this investigation is negligible since a maximum displacement of one half the probe diameter is small compared to the wake width and the shear gradient is small.

III. EXPERIMENTAL WORK

Apparatus Used in the Experimental Work

Inducer

To improve the suction specific speed of centrifugal impellers used in rockets and missiles, an axial flow inducer is usually employed upstream of the primary pump. The inducer test facility (built for the purpose of studying the secondary flow phenomena) was employed for the purpose of correlating the results of rotating and stationary pressure probe measurements. The inducer test facility is shown in Figure 1. The inducer has an unusually long fluid passage and hence fluid friction effects dominate the whole flow field and cause considerable deviation in the flow from the design values. The inducer was designed by G. F. Wislicenus and B. Lakshminarayana (7), using the Wislicenus (8) method based on mean streamline considerations. Important parameters of the inducer are as follows:

Number of blades	=	4
Hub/tip ratio (outlet)	=	0.5
Tip diameter	=	36.0 inches
Design value of flow coefficient (inlet)	=	0.065
Blade tip velocity for this study	=	71.4 feet/second
Blade chord		
Tip section	=	82.96 inches
Mid-span	=	63.18 inches
Hub	=	49.94 inches

Rotating Probe Holder

The static and total pressure distributions of the relative flow were obtained with the aid of a rotating pressure probe holder and a

pressure transfer device. The rotating probe holder will be discussed in this section and the pressure transfer device will be described in the following section.

The probe holder, shown in Figure 2, is an aluminum cylindrical disk and was fastened to the inducer rotor one inch behind the trailing edge of the hub blade section as is shown in Figure 4. The probe holder was designed for obtaining pressure measurements across two blade passages, which are 180 degrees apart. Each half of the holder contains twenty-two probe receptacles which serve to anchor the probes and to transmit the pressure from the probe, through connecting tubing, to the pressure transfer device.

The twenty-two probe receptacles were spaced along a circumferential arc of 130 degrees as is shown in Figure 3. Nine receptacles, spaced five degrees apart, comprise both ends of this 130 degree survey span and the other four receptacles were equally spaced in the remaining 50 degree span. Although the blade interval spans a 90 degree arc, extra receptacles were included to obtain measurements in the wakes of the blades which form the flow passage. In the presentation of the experimental data, the blade intervals have been clearly indicated.

Pressure Transfer Device

The pressure transfer device was designed to transmit the static and total pressures of the relative flow from the rotating probes to a stationary manometer. The pressure from the rotating probes is transmitted through the probe holder, attached to the rotor, to the outer housing of the pressure transfer device shown in Figure 5. The

pressure was then transmitted to stationary pressure leads, inside a hollow shaft, through an annular space formed by the outer housing and the stationary shaft. The annular spaces were sealed by means of rubber rings.

As a check of the accuracy of the pressure transfer device, a stationary total pressure probe was placed in the axial direction just in front of the blade row. To this measured absolute inlet total pressure was added the component of the dynamic pressure which was associated with the blade speed for the given radial position. This relative flow inlet total pressure was compared with the corresponding measured total pressure obtained from a rotating total pressure probe located approximately at the same axial and radial station. After correcting the rotating probe total pressure measurement for the centrifugal force effect, the two values of the relative flow inlet total pressure were very close. The pressure transfer device was also checked for leakage between the two chambers.

Instruments Used in Experimental Work

Total Pressure Probe

A wide variety of total pressure probe designs has been experimentally investigated by Gracey (9) to determine the effect of the flow angle of attack upon the pressure sensed by the probes over a Mach number range from 0.26 to 1.62. The results of Gracey's investigation are presented in terms of the sensitivity range. The sensitivity range is defined as the angular range at which the total pressure error reaches a value of one per cent of the true impact pressure.

Gracey's results showed that for simple, non-shielded probes, the sensitivity range was found to depend on the external shape of the nose section, the size of the impact opening (relative to the tube diameter), and the shape of the internal chamber behind the impact opening. The best combination of these design features (that is, a tube having a cylindrical nose shape, an impact opening equal to the tube diameter, and a 30 degree conical chamber) produced the highest sensitivity range (about 28 degrees at Mach number of 0.26) of any of the non-shielded tubes.

The original design of the total pressure probes used in this investigation was based upon Gracey's conclusions. The outside diameter of the total pressure probes was 0.125 inches and the inside diameter was 0.055 inches. The lowest Mach number considered by Gracey was considerably higher than the Mach numbers expected to be encountered in this investigation. This made it necessary to check upon Gracey's design conditions. It was found that for a flow with a Mach number of 0.045, an internal chamber with a cone angle of 60 degrees gave the highest sensitivity range. The sensitivity range was found to be ± 18 degrees and the probe calibration curve is given in Figure 6.

Static Pressure Probe

A standard static pressure probe was used to obtain the absolute flow static pressure measurements for the three radial positions. The probe had a cylindrical stem with a diameter of 0.040 inches. Four static holes, each having a diameter of 0.010 inches, were spaced 90

degrees apart around the stem circumference. The static holes were located 0.20 inches from the probe nose.

When the static pressure probe was not aligned in the direction of the oncoming flow, its reading was higher than the true static pressure. In order to correct for the increased pressure reading due to the addition of a dynamic component of pressure, it was necessary to calibrate the probe. This was accomplished by plotting the difference between the measured and true static pressure divided by the dynamic pressure of the flow against the angle which the probe made with the flow direction $\left[\frac{P_s - P_{s_{\lambda=0}}}{q} \text{ v.s. } \lambda\right]$. For the static pressure probe used in this investigation, the calibration curve is as shown in Figure 7.

Wedge Probe

A wedge probe was used in this investigation to obtain both the relative flow static pressure distribution and the relative flow discharge angles along the circumferential direction. The flow angles and static pressure distributions were obtained for the three radial positions (r/r_t = 0.975, 0.777, 0.55).

The wedge probe had an included angle of 5.5 degrees and the wedge faces were 0.30 inches long and 0.120 inches in height. The static pressure holes on the wedge faces were 0.015 inches in diameter and located 0.20 inches behind the probe leading edge.

The wedge probe was calibrated for flow angle measurements. This was accomplished by plotting the pressure differential acting upon the wedge faces divided by the dynamic pressure of the flow against

the angle which the probe made with the oncoming flow $\left[\frac{\Delta P_w}{q} \text{ v.s. } \lambda\right]$. The wedge probe calibration curve is given in Figure 8.

The wedge probe was also used for relative flow static pressure measurements. The probe was rotated until $\Delta P_w = 0$ and the pressure acting on one of the faces was recorded. In this case, since the wedge face was not parallel to the flow (deviation angle = 2.7 degrees), the probe holes read the static pressure plus a component of the dynamic pressure. It was found that in the case of a uniform flow with a velocity of 42 feet per second*, the static pressure recorded by the wedge probe was larger than the true static pressure by eight per cent of the flow dynamic pressure.

Manometer Characteristics

A micromanometer, manufactured by Flow Corporation, was used to obtain the pressure measurements in the investigation. Water was used as the manometer liquid. In use, the height of a glass tube containing the manometer fluid was adjusted until the liquid meniscus was restored to the position it occupied before the unknown pressure difference was applied. The vertical displacement of this tube required to restore the meniscus to its known position was read with a vernier micrometer calibrated directly in 0.0001 inch increments. The accuracy of the micromanometer is $\pm$ 0.09 per cent of the minimum static pressure measured by the rotating wedge probe in this particular experiment.

---

* This velocity and the relative velocity of the inducer are of the same order of magnitude.

Experimental Procedure

The experimental portion of this investigation was directed towards obtaining the static pressure, total pressure, discharge flow angle, and velocity distributions of the relative flow across one of the blade passages. The absolute flow static and total pressures were also obtained experimentally for the same axial station and three radial positions. The radial positions were 1, 5 and 8 1/2 inches from the inducer hub (r/r_t = 0.55, 0.77 and 0.97, respectively).

A very thin (0.003 inches thick) brass flag mounted on the tip of the rotating total pressure probe was used to align the probe in the relative flow direction. The alignment of the rotating total pressure probe with the directional flag was accomplished with the aid of a stroboscope high intensity flash lamp. For each circumferential and radial position, the total pressure probe was aligned in the flow direction. Since the probe length was constant and the relative flow angles were varying across the blade passage for the tip and mid-radius locations, the axial distance from the blade trailing edge to the probe inlet was also varying across the blade passage. As shown in Figure 12, the relative flow angles variation was not large and the axial location of the total pressure probes as shown in Figure 4 was based upon the spacial average relative flow discharge angle to be discussed later.

The relative flow static pressure, discharge flow angle, and velocity distributions across one of the blade passages were obtained by using a wedge probe. The wedge probe had an included angle of 5.5 degrees and was described earlier.

The wedge probe was mounted to the probe holder disk behind the rotating blade system. The probe was then turned until the pressure differential acting upon the wedge faces vanished (i.e. bisector of the wedge angle aligned in flow direction). Upon disconnecting one of the manometer leads, it was then possible to measure the static pressure for that given circumferential and radial location. It should be noted that preliminary wind tunnel tests have shown that the static pressure reading obtained in this manner was larger than the true static pressure by eight per cent of the flow dynamic pressure. This correction was applied to all the measurements obtained from wedge probe. The wedge probe was used only to obtain the static pressure measurements for the tip and mid-radius locations. The hub static pressure measurements were obtained from rotating wall taps located flush with the rotating probe holder disk. As a check to see if the wedge probe gave reasonable static pressure measurements, the spacial average static pressure measurements, to be discussed later, were compared with a theoretical curve based upon radial equilibrium and wall static pressure measurements obtained 1.5 inches downstream of the rotating probe holder disk. This comparison of static pressures is shown in Figure 15.

In order to obtain the relative flow direction, it was necessary to first obtain the relative flow velocity for the given position. This was accomplished by applying the centrifugal force correction to the total and static pressures previously obtained. To obtain the relative flow direction, the wedge probe was placed in the tangential direction and the pressure differential acting upon the wedge faces

was recorded. Knowing this pressure differential and the relative flow velocity for the particular position, the wedge probe calibration curve was used to obtain the flow angle with respect to the tangential direction. In order to check the accuracy of the wedge probe calibration curve, the wedge probe for a mid-radius location was rotated about its vertical axis until the pressures acting upon both of the wedge faces were the same ($\Delta P_w = 0$). The direction of the probe with respect to the tangential direction corresponded with the value obtained by using the wedge probe calibration curve as described above.

Possibly large flow interference effects produced by the wedge probe holder and connecting tubing made it necessary to abandon wedge probe measurements for the hub location ($r/r_t = 0.55$). The directional flag mounted on the rotating total pressure probes indicated that the relative discharge flow was in the tangential direction for the hub location. Absolute flow angle measurements, to be discussed later, indicated that the absolute flow was in the tangential direction.

The static and total pressures of the absolute flow were obtained in the following manner. A conventional static pressure probe was placed in the absolute flow field at the same axial station and radial position as the rotating probes. The static pressure probe was rotated until the minimum pressure was obtained. This pressure was the static pressure of the absolute flow field and the probe angle and was used for aligning the stationary total pressure probe. After aligning the stationary total pressure probe with the angle previously determined, the total pressure of the absolute flow field was determined. It should be noted that the length of the stationary total

pressure probe was determined after the probe was placed in the direction of the absolute flow. This was done to insure that both the rotating and stationary total pressure measurements were obtained at the same axial location. The absolute flow angle measurements are discussed in the section dealing with the discharge flow angles and velocity triangles.

Experimental Results

Rotating Probe Measurements

In order to correlate the rotating and stationary total pressure measurements, it was necessary to convert the total pressure of the relative flow ($p_s + 1/2\ \rho\ W^2$) to an absolute frame of reference and derive the equivalent total pressure of the absolute flow ($p_s + 1/2\ \rho\ V^2$). The total pressure data was expressed as an equivalent non-dimensional absolute total pressure distribution by means of the following equation:

$$\psi_{T_{ab}} = \frac{2gH_R}{U_t^2} + \left[\left(\frac{V_\theta}{U_t}\right)^2 - \left(\frac{W_\theta}{U_t}\right)^2\right] \qquad (19)$$

where

$\psi_{T_{ab}}$	is the non-dimensional total pressure of the absolute flow
H_R	is the gage total pressure of the relative flow
U_t	is the blade tip velocity
V_θ	is the tangential component of the absolute discharge velocity
W_θ	is the tangential component of the relative discharge velocity

The circumferential variation of the absolute total pressure coefficient ($\psi_{T_{ab}}$) was plotted for the three radial positions and is shown in Figure 9. The blade intervals are clearly indicated on the graph and the spacial average for each absolute total pressure coefficient ($\bar{\psi}_{T_{ab}}$) was obtained over the blade interval. These values for the three radial positions were correlated with the stationary probe measurements.

The static pressure distribution is the same in relative and absolute flow for a given axial and radial position. The non-dimensional static pressure coefficient is given as follows:

$$\psi_s = \frac{2gh_s}{U_t^2} \tag{20}$$

where

ψ_s is the non-dimensional static pressure coefficient

h_s is the relative flow gage static pressure

U_t is the blade tip velocity

After correcting for the error due to the wedge probe picking up a component of the dynamic pressure, the circumferential variation of the static pressure coefficient (ψ_s) was plotted for the three radial positions and is shown in Figure 10. The blade intervals are clearly indicated on the above graph and the spacial average of each static pressure coefficient ($\bar{\psi}_s$) was obtained over the blade interval. These values for the three radial positions were correlated with the stationary probe measurements.

Stationary Probe Measurements

The stationary probe static and total pressure measurements were obtained using the procedure described previously. The stationary probe total pressure measurements ($\Psi_{T_{ab}}$) for the three radial positions were compared with the corresponding spacial averages of the total pressure distribution ($\bar{\Psi}_{T_{ab}}$) for one blade passage and is shown in Figure 11. The stationary probe static pressure measurements (Ψ_S) for the three radial positions were compared with the corresponding spacial averages of the static pressure distribution ($\bar{\Psi}_S$) for one blade passage and is shown in Figure 11. Using the value of the rotating probe measurements as the base, the per cent error for the six measurements is shown in Figure 11. It should be noted that a positive per cent error means that the stationary probe measurement was larger than the spacial average value. A detailed discussion of the errors is dealt with in the next chapter.

Discharge Flow Angles and Velocity Triangles

The circumferential variation and spacial average over one blade passage of the relative flow discharge angles (β) from the tangential direction for the three radial positions is shown in Figure 12. The spacial average relative flow discharge angle is compared to the design blade angles at the trailing edge and is shown in Figure 16. After correcting the static pressure measurements, due to the wedge probe picking up a component of the dynamic pressure, the spacial average of the relative discharge velocities was obtained for each of the three radial positions. These values, along with the spacial

average of the relative flow discharge angles, were used to determine the inducer discharge flow velocity triangles for the three radial positions and is shown in Figure 13. Included in Figure 13 are the discharge velocity triangles based upon absolute flow measurements for the same axial and radial location and the design discharge velocity triangles are also given. A discussion of the difference between the discharge velocity triangles derived from relative flow measurements and those derived from absolute flow measurements is presented in the next chapter.

The discharge flow angles of the absolute flow derived from the wedge probe was compared with the measurements obtained from a stationary claw probe located approximately at the same axial station and is shown in Figure 14. Since the circumferential variations of the discharge angles were not large, a claw probe would give meaningful information. A critical comparison of the result and a discussion of the errors in angle and static pressure measurements obtained from the wedge probe is given in the next chapter.

IV. DISCUSSION AND CONCLUSIONS

The manometer fluctuation about the fluid level corresponding to the time average input pressure was shown to be the particular solution of the differential equation governing the manometer response. For a sinusoidal input pressure fluctuation, the manometer response was shown to depend upon the value of $\frac{4L\omega^2}{3g}$, where (L) is the total length of manometer fluid corresponding to the time average input pressure and (ω) is the angular frequency of the pressure fluctuation.

For the inducer considered in this investigation, the maximum pressure fluctuation was produced by the blade tip section (r/r_t = 0.975) and is shown in Figure 9. In order to obtain an estimate of the manometer response, the total pressure fluctuation produced by the blade tip section was represented by a sine wave with an amplitude of approximately 0.075 inches of water and a frequency of 30.33 cycles per second. The total length of manometer fluid (L) corresponding to the time average input pressure was approximately one foot. Neglecting the effect of the connecting tubing, equation (15) was used to calculate the amplitude of the manometer fluctuation which was found to be .0004 inches of water. The predicted amplitude of the manometer fluctuation was very small and cannot be detected by the manometer used in this investigation. This agrees with the observed behavior of the manometer liquid column.

Generally speaking, it is possible to approximate a periodic input pressure fluctuation by a sinusoidal or group of sinusoidal

pressure waves. It can be concluded that for small pressure fluctuations compared to the time average value of the input pressure, and when $\frac{4L\omega^2}{3g} >> 1$, the amplitude of the manometer fluctuation will approach zero and the manometer will record the time average value of the input pressure fluctuation.

The comparison between the stationary probe static pressure measurements and the spacial average static pressure measurements obtained over one blade passage is presented in Figure 11. The reasons for the difference in measurements for the tip and mid-radius locations are as follows: (1) the variation in discharge flow direction caused the conventional stationary static pressure probe to record a component of the dynamic pressure; (2) depending upon the frequency and amplitude of the fluctuating pressure and the probe characteristics, the stationary static pressure may register a pressure which is different from the time average static pressure; (3) neglecting the variation of the turbulence level across the blade passage, the suspected high turbulence level had a greater influence upon the stationary probe than upon the rotating wedge probe; (4) the stationary static pressure probe was exposed to all four blade wakes whereas the spacial average static pressure obtained from the rotating wedge probe was based on one blade passage. If the flow in all four blade passages was not identical, an additional error was introduced in the stationary static pressure measurements; and (5) since the static pressure rise was very small, any experimental error would have a significant effect upon the pressure measurements.

The extent to which the above error producing effects are interrelated and the lack of quantitative information concerning the

turbulence level make it impossible to discuss the various reasons for the observed difference in static pressure readings to any extent.

Rotating wall static pressure taps were used to obtain the relative flow static pressure variation for the hub location. As could be expected, the agreement between the hub spacial average static pressure and the stationary probe static pressure measurement was better than the agreement obtained for the tip and mid-radius locations.

A major conclusion to be derived from this investigation is that in turbomachinery research, where the flow directional variation and turbulence level are significant, the conventional static pressure probe located in the absolute flow field will record a pressure greater than the time average static pressure.

The comparison between the stationary probe total pressure measurements and the absolute flow total pressure measurements derived from rotating probes and averaged over one blade passage is presented in Figure 11. The comparison between the absolute flow discharge angles derived from relative flow measurements and those obtained from the stationary claw probe is presented in Figure 14. The large difference in the total pressure coefficients ($\psi_{T_{ab}}$) and absolute discharge flow angles (α) derived from the rotating probe measurement and those obtained from stationary measurements at the tip and mid-radius location is due to inaccuracies of the wedge probe used for measuring the static pressure and flow discharge angles of the relative flow. The wedge probe calibration curve is shown in Figure 8, and for angles of attack larger than ten degrees the effect

of flow separation on the wedge faces was likely to introduce inaccuracies in the flow angle measurements.

Any error in calculating the velocity vectors of the relative flow due to incorrect static pressure and flow angle measurements is greatly magnified by equation (19). This expression was used to convert the relative flow total pressure measurements to the absolute reference frame. An example to show the magnification of small experimental errors is as follows: for the non-symmetric mid-radius velocity triangle shown in Figure 13, the spacial average relative flow velocity was increased by five per cent. As a result of this change the absolute flow total pressure coefficient ($\bar{\psi}_{T_{ab}}$), derived from the relative flow measurements, was decreased by 14.1 per cent and the derived absolute flow discharge angle was increased by 16.4 per cent. Small experimental errors in the measurement of the relative flow discharge angle would have a similar effect. Knowing that small experimental errors are greatly magnified, the agreement between the stationary probe total pressure measurements and the spacial average total pressures derived from rotating probe measurements for the tip and mid-radius locations is considered good.

As was described previously, rotating wall static pressure taps were used to obtain the relative flow static pressure variation for the hub location and the relative discharge flow direction was shown to be in the tangential direction. As a result, the calculations for the velocity variation of the relative flow were accurate and good agreement between the stationary probe total pressure measurement and the spacial average total pressure derived from rotating probe measurements was obtained as is shown in Figure 11.

A major conclusion to be derived from this investigation is that if the pressure fluctuation is small compared to the time average pressure and the variation in flow direction is less than the probe sensitivity range, the error between the measured total pressure and the time average total pressure is small.

The inducer design velocity triangles, the velocity triangles based upon relative flow measurements, and the velocity triangles based upon the absolute flow total pressure and discharge angles and static pressure derived from wall static pressure taps is shown in Figure 13. From the above discussion on the magnification of experimental errors, the discrepancies between the stationary claw probe measurements of the absolute flow discharge angles and those angles derived from the relative flow measurements is not as overwhelming as first it would appear. As mentioned above, these discrepancies in absolute flow angles as well as absolute flow velocities can be traced back to inaccuracies of the rotating wedge probe used in measuring the static pressure and discharge flow angles of the relative flow.

The major conclusion derived from this investigation is as follows: (1) if the input pressure fluctuation is small compared to the time average pressure, the manometer would register the time average input pressure; (2) for flow fields which vary in direction and have a high turbulence level, static pressure probe measurements are very inaccurate; (3) if the total pressure fluctuation is small compared to the time average total pressure and the flow angle variation is less than the probe sensitivity range, the error between the measured total pressure and the time average total pressure is small.

BIBLIOGRAPHY

1. Schlichting, H., Boundary Layer Theory, McGraw-Hill Book Co., Inc., New York, p. 574 (1960).

2. Lakshminarayana, B., J. H. Horlock, "Effect of Shear Flows on the Outlet Angle in Axial Compressor Cascades - Methods of Prediction and Correlation with Experiments," J. of Basic Engr., Trans. ASME, Series D, Vol. 89, p. 191 (March 1967).

3. Goldstein, S., Modern Developments in Fluid Dynamics, Dover Publications, Inc., New York, Vol. I, p. 253 (1965).

4. Bramwell, Relf, and Fage, A.R.C., Reports and Memoranda, No. 71.

5. Doebelin, E. O., Measurement Systems: Application and Design, McGraw-Hill Co., Inc., New York, p. 373 (1966).

6. Lighthill, M. J., "Contributions to the Theory of the Pitot-Tube Displacement Effect," J. of Fluid Mech., Vol. 2, p. 493 (1957).

7. Wislicenus, G. F., B. Lakshminaryana, "Design of a Test Inducer," Interim Report submitted to NASA, NsG 573, (March 1964).

8. Wislicenus, G. F., Fluid Mechanics of Turbomachinery, Dover Publications, Inc., New York, Vol. II, Chp. 29 (1965).

9. Gracey, W., "Wind Tunnel Investigation of a Number of Total Pressure Tubes at High Angles of Attack, Subsonic, Transonic, and Supersonic Speeds," NACA Report 1303 (1957).

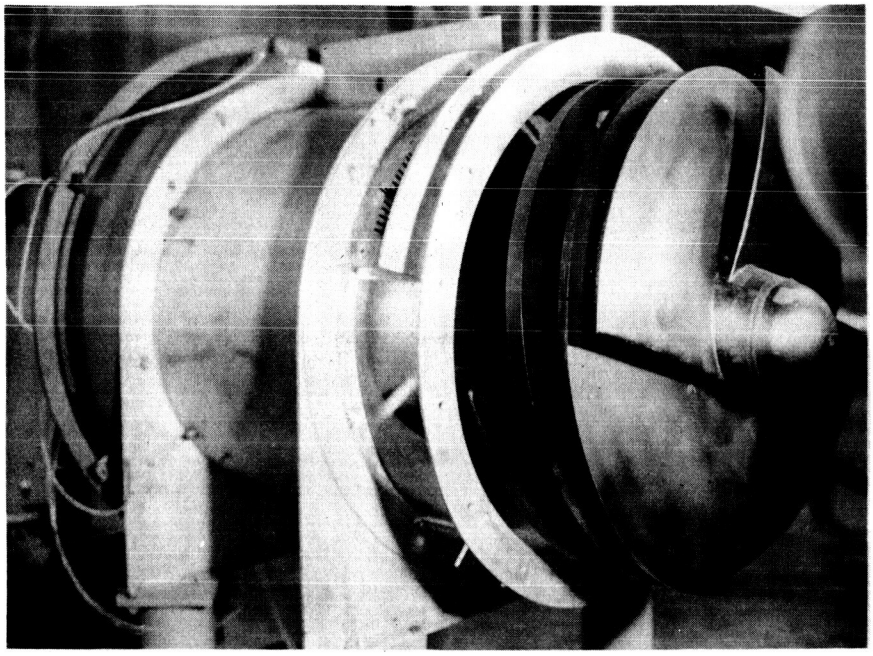

Inducer with shroud removed

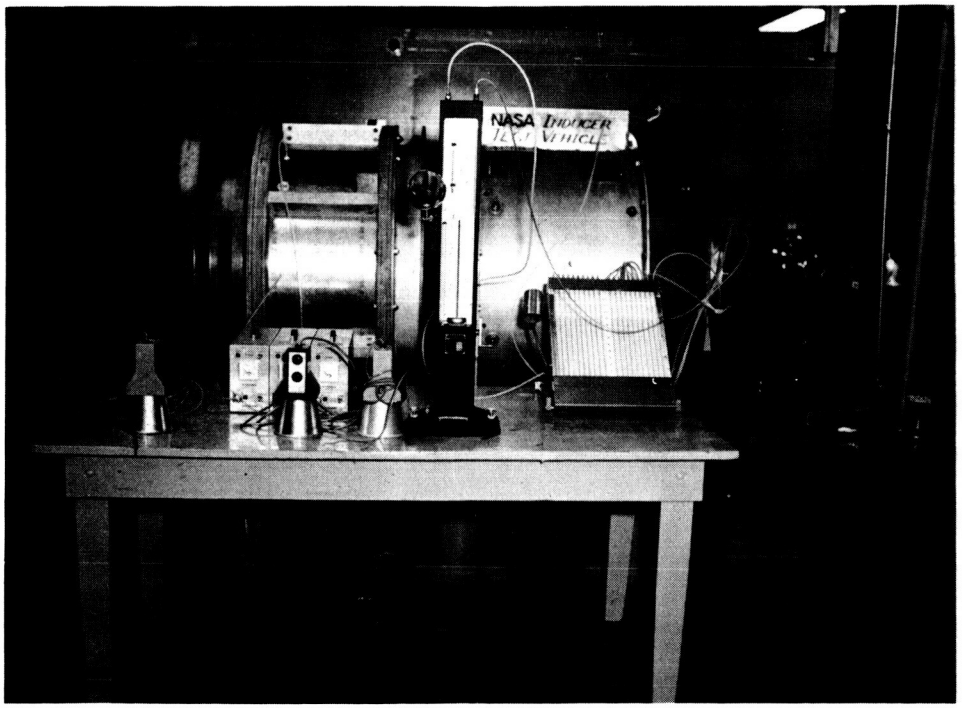

Test assembly

Figure 1: Experimental Inducer Model

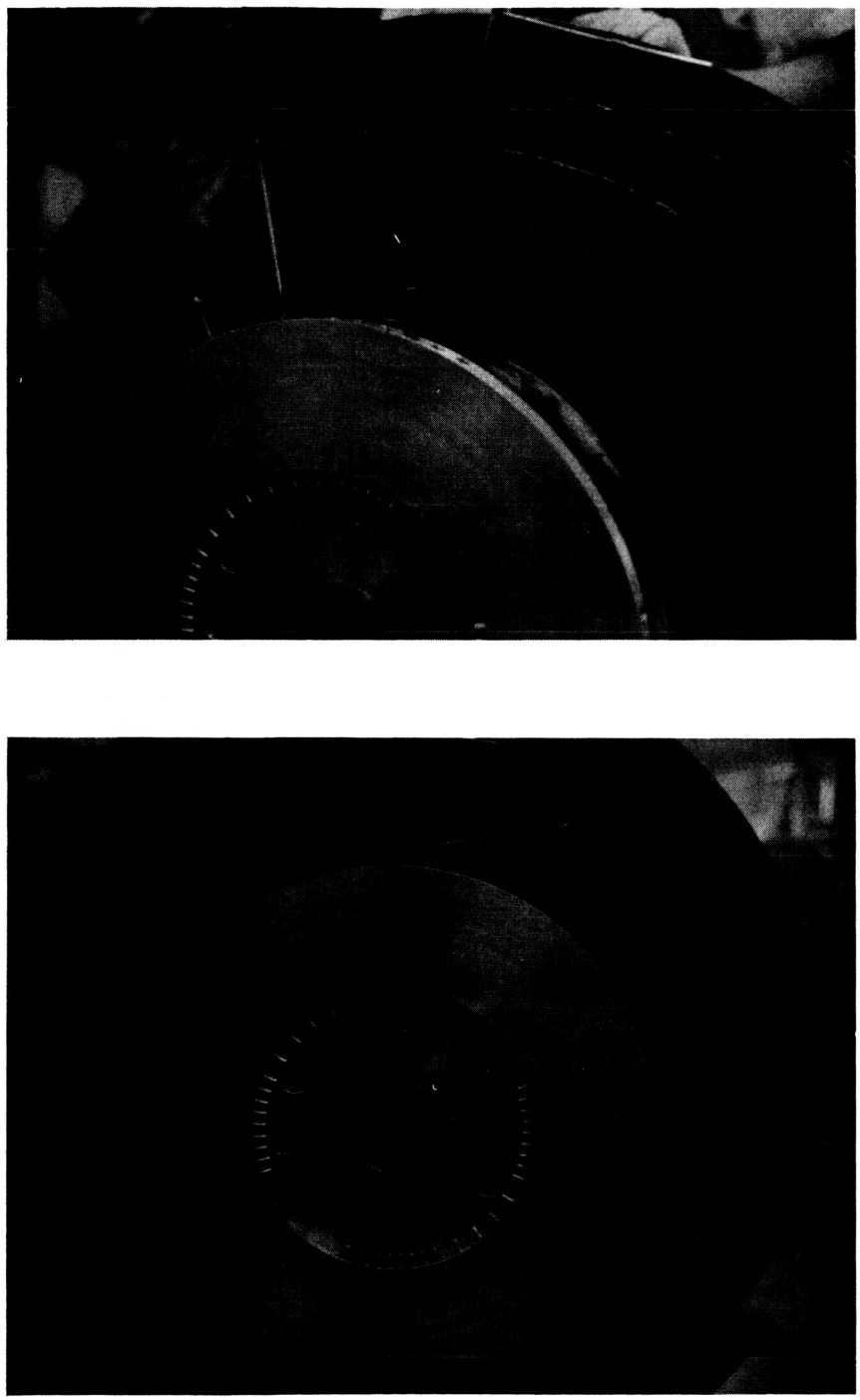

Figure 2: Photographs of Rotating Pressure Probe Holder

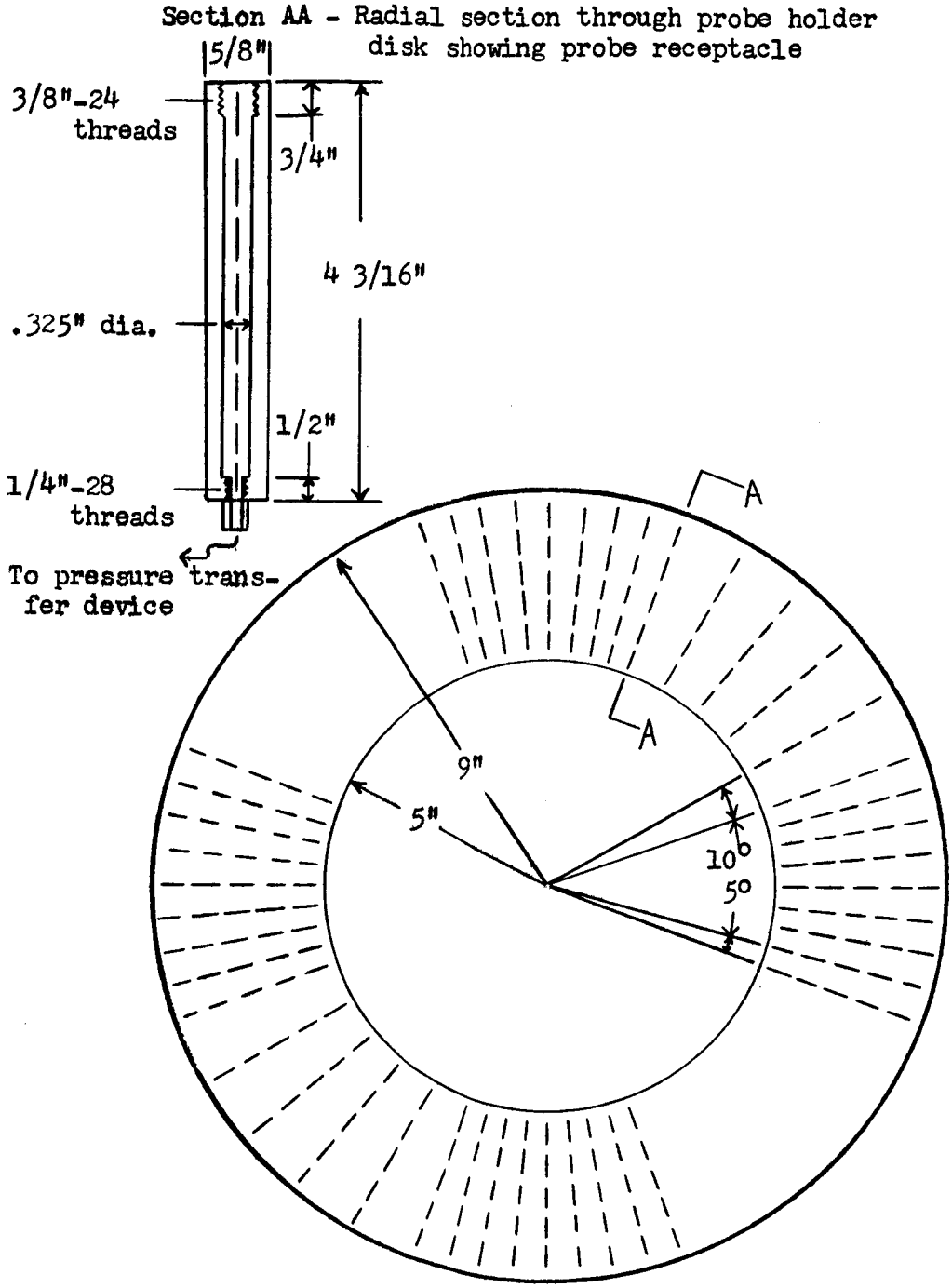

Figure 3: Detailed Drawing of Rotating Pressure Probe Holder

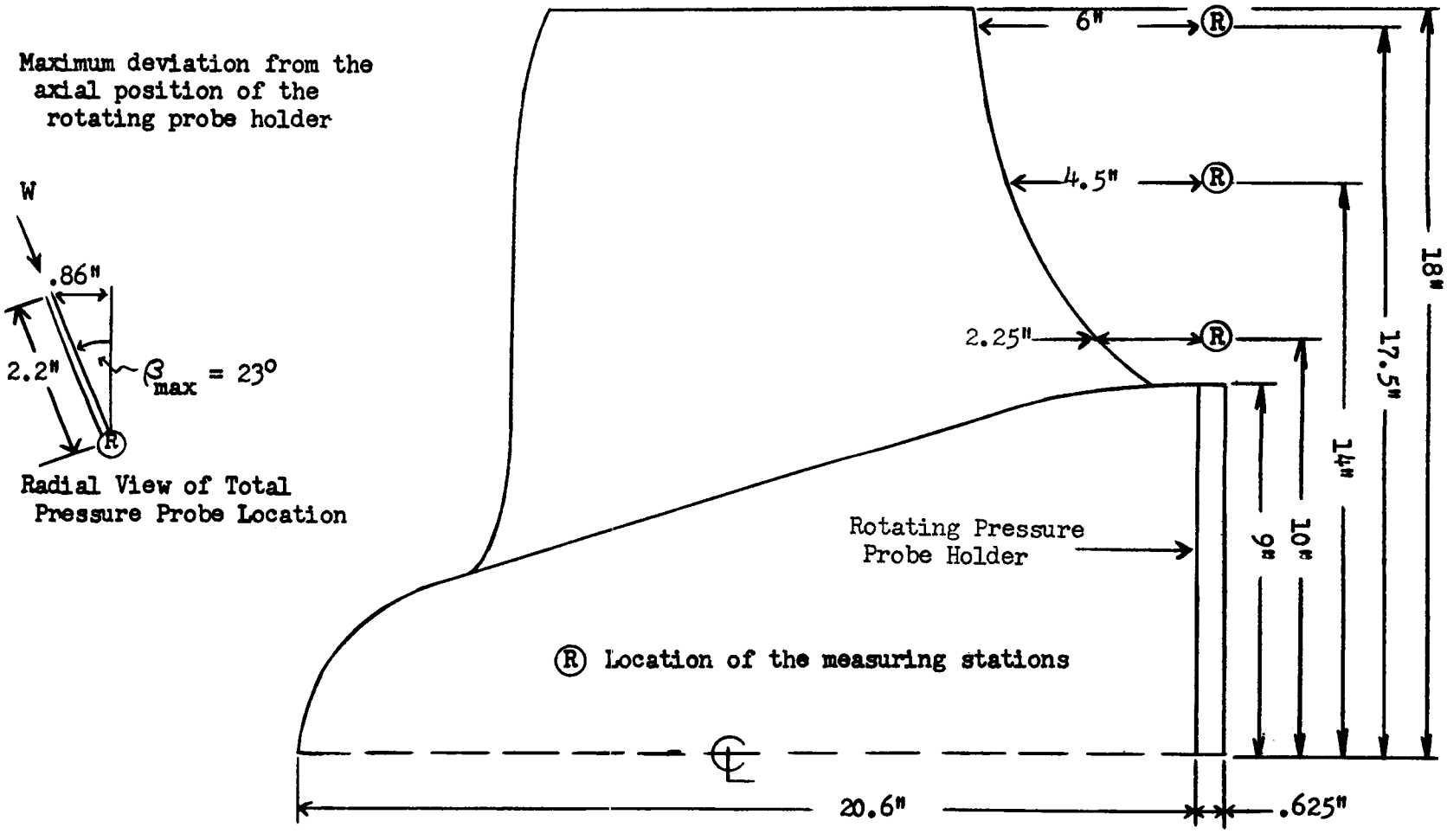

Figure 4: Location of the Rotating Pressure Probe Holder and Measuring Stations

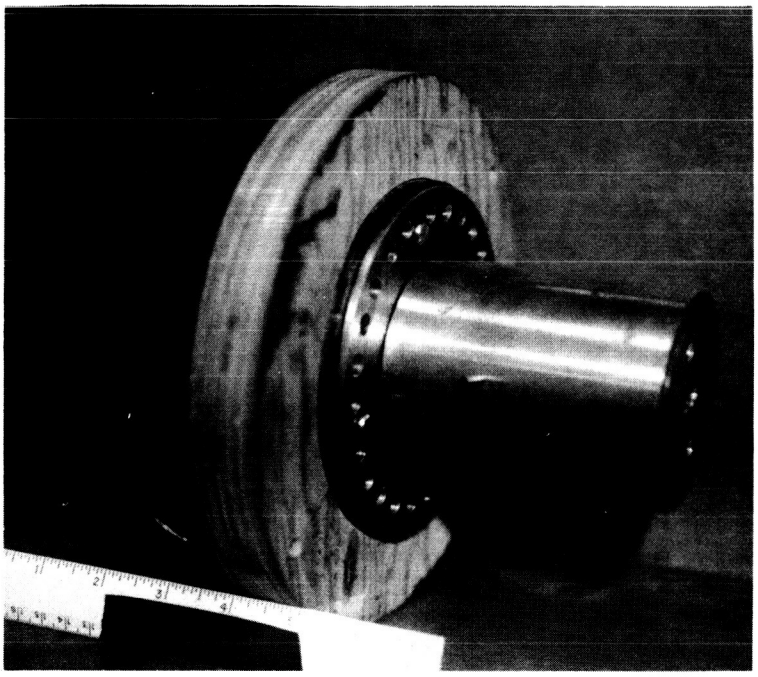

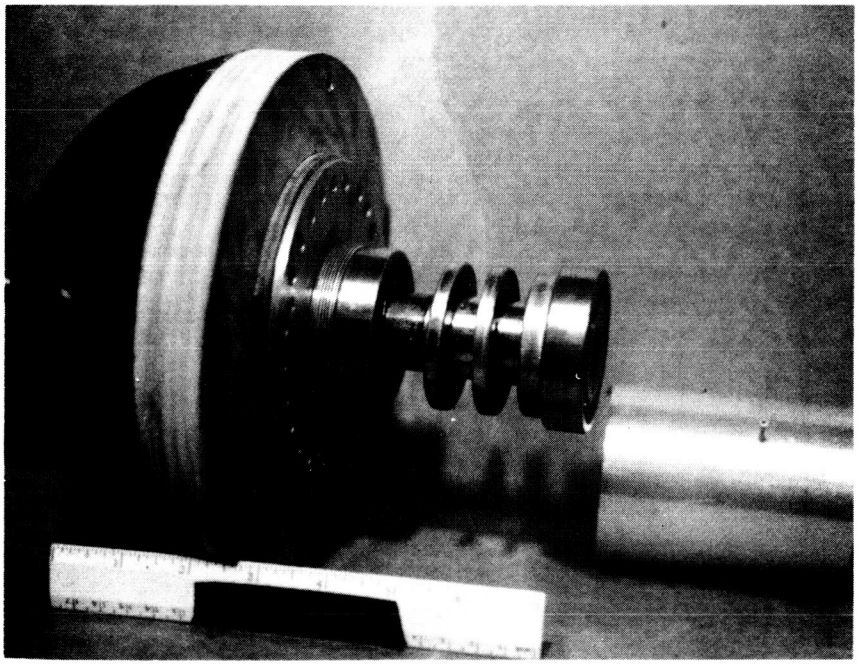

Figure 5: Photographs of the Pressure Transfer Device

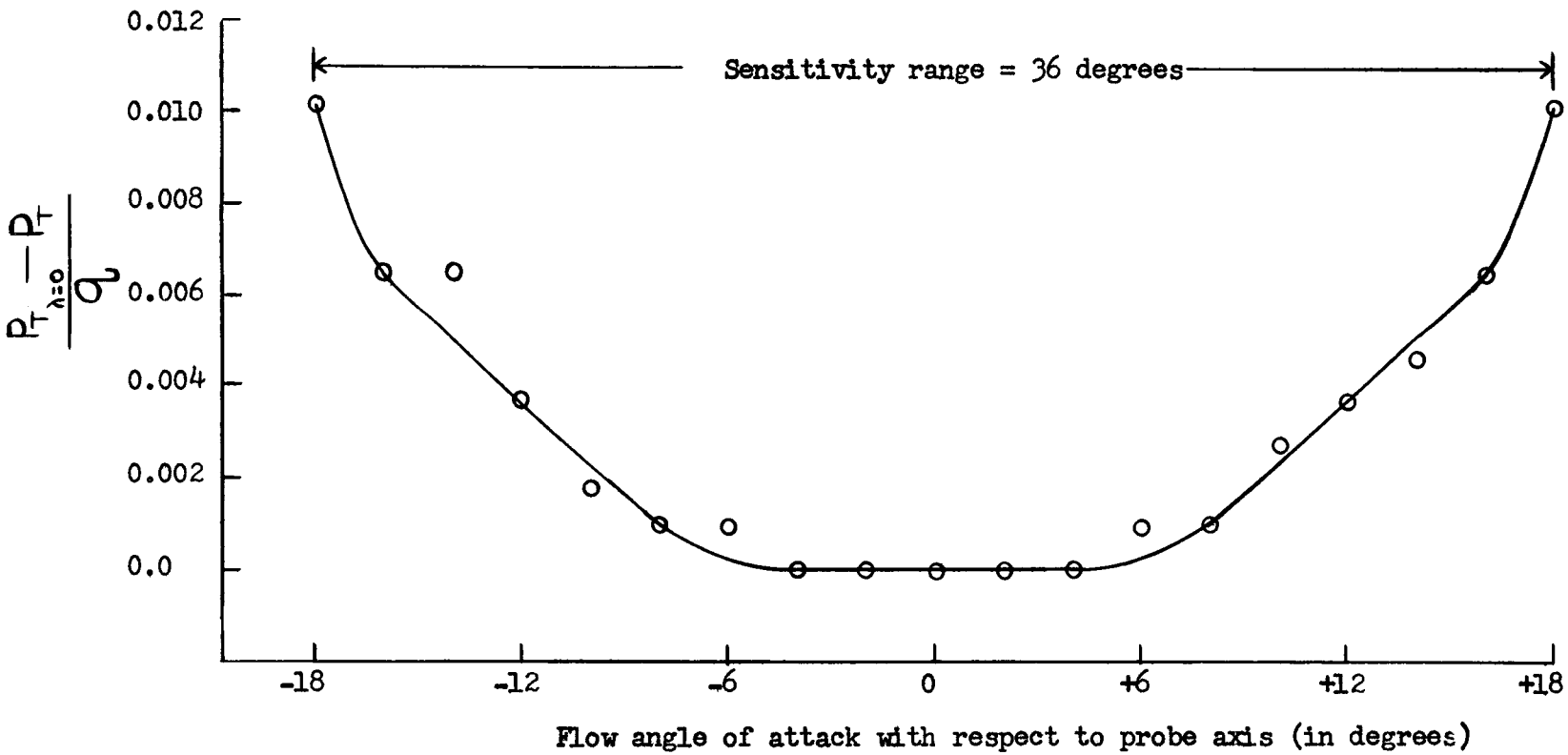

Figure 6: Total Pressure Probe Calibration Curve

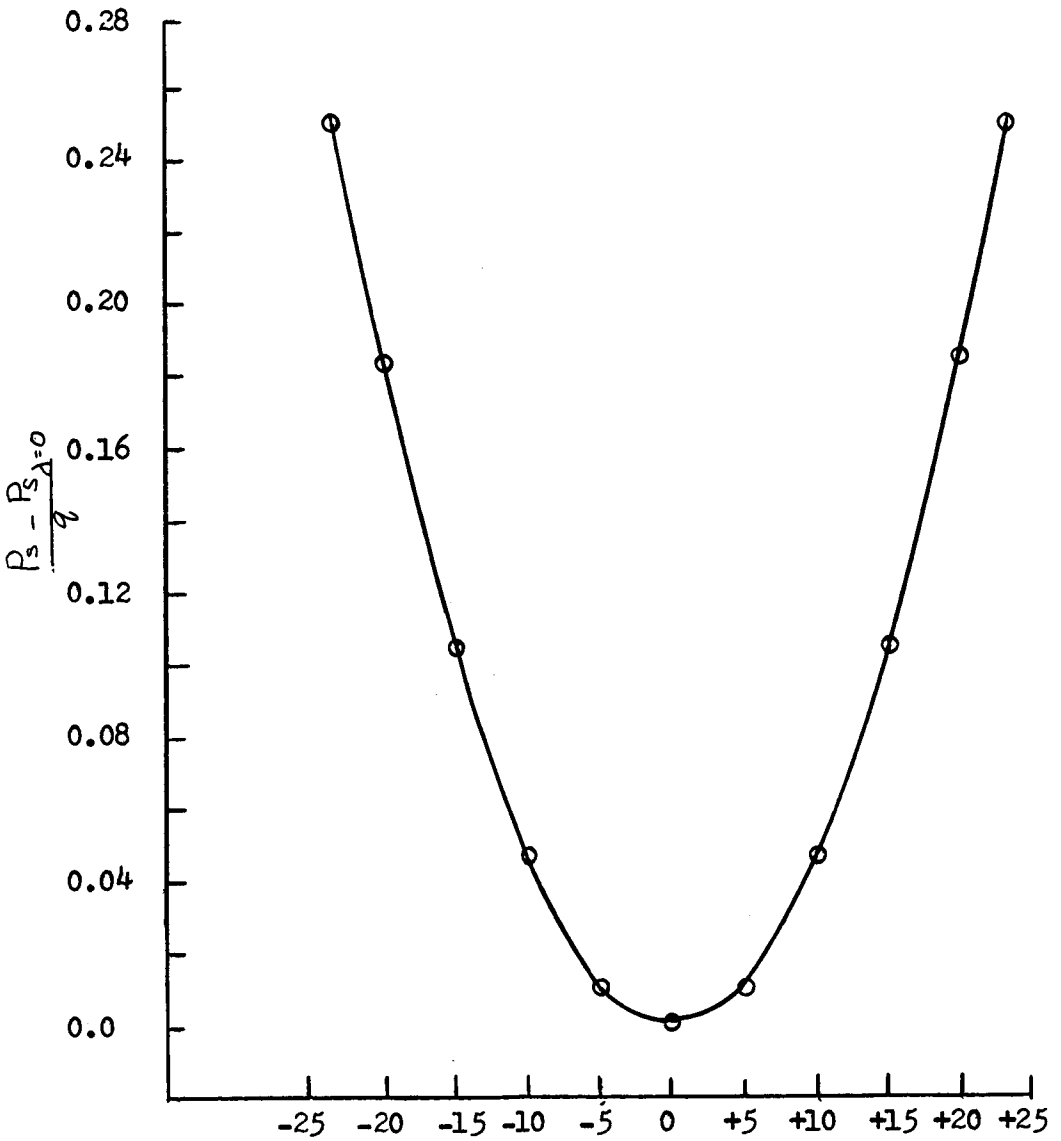

Figure 7: Static Pressure Probe Calibration Curve

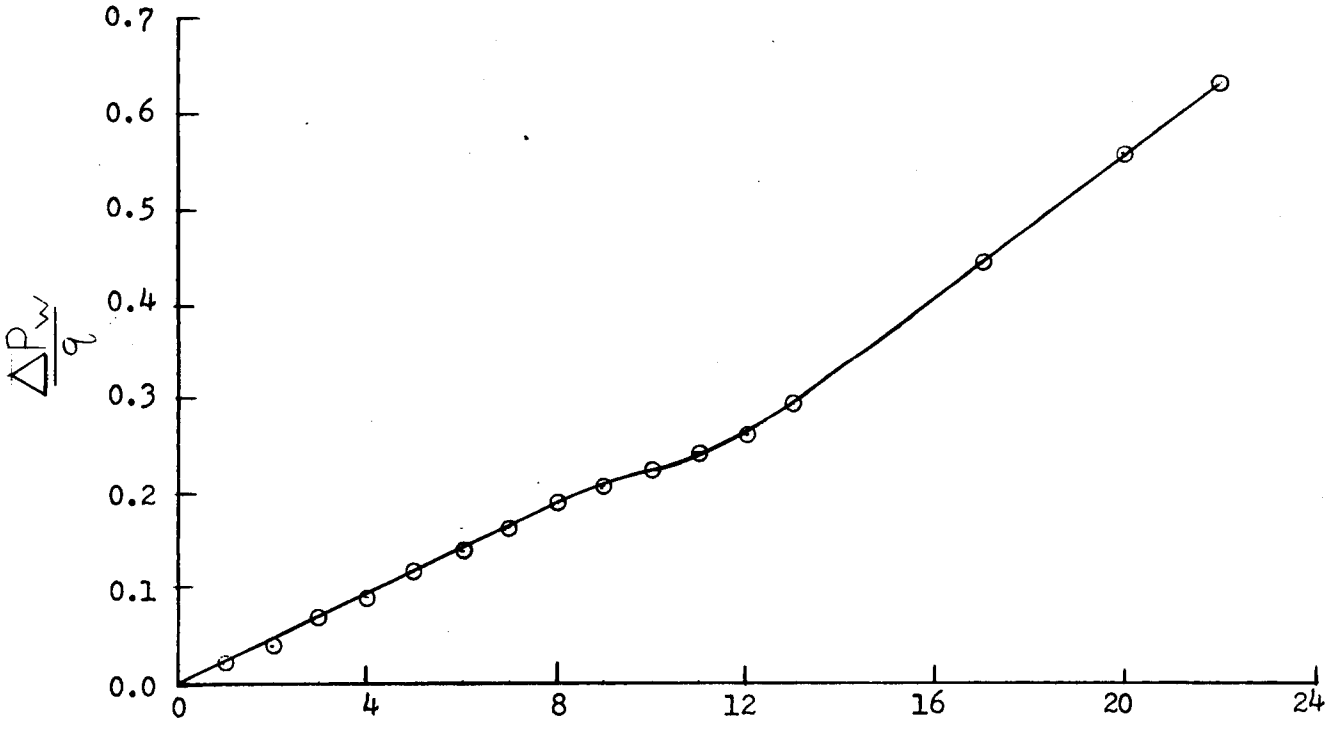

Figure 8: Wedge Probe Calibration Curve

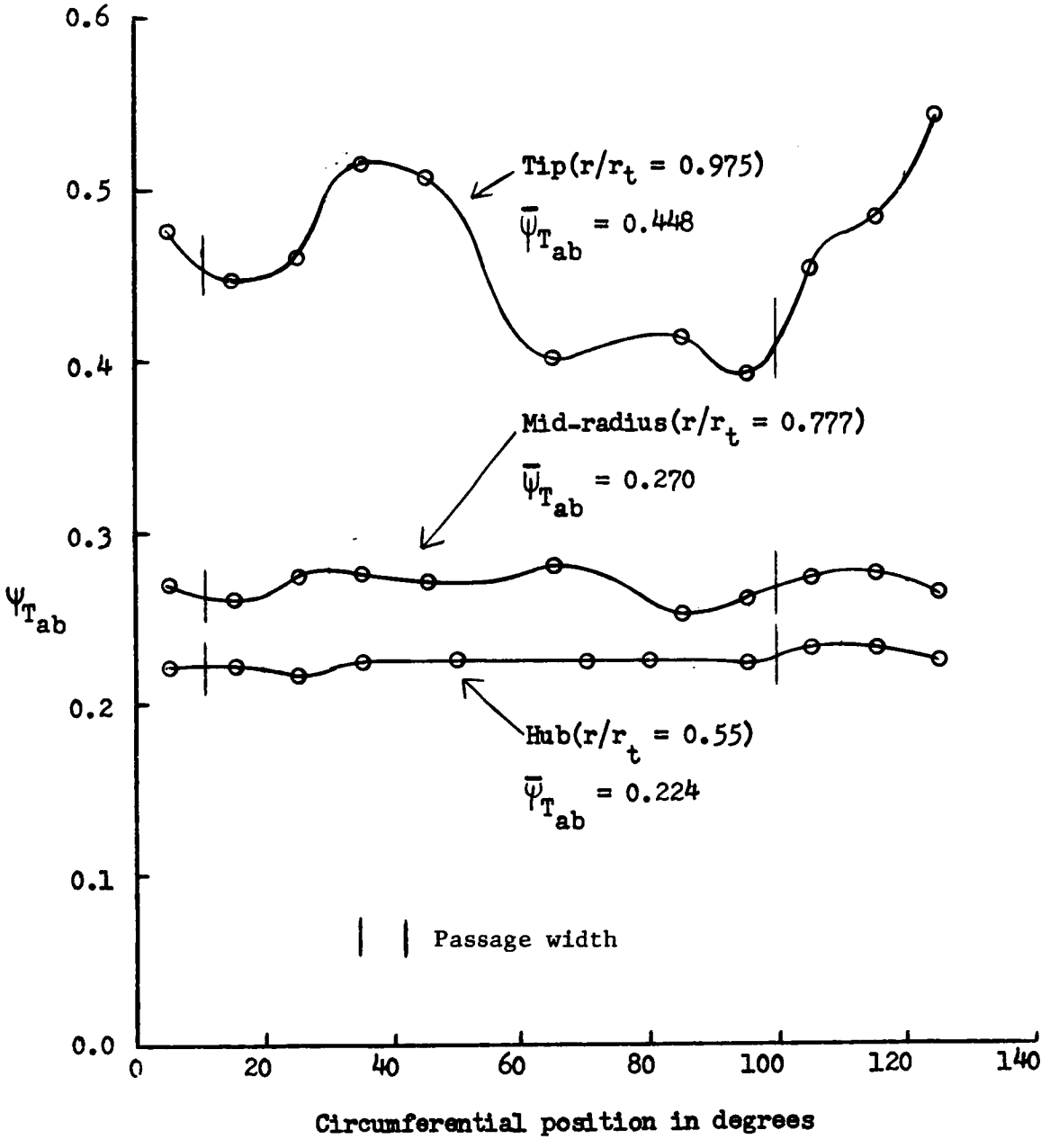

Figure 9: Circumferential Distribution of the Absolute Flow Total Pressure Coefficient

The data given in Fig. 10 are based on the static pressure measurement obtained with a rotating wedge probe at tip and midradius and with rotating wall piezometor holes at the root. The fact that ψ_s at the root is slightly higher than at the midradius indicates clearly that the pressure readings are in error at least at the mid-radius. See Fig. 15.

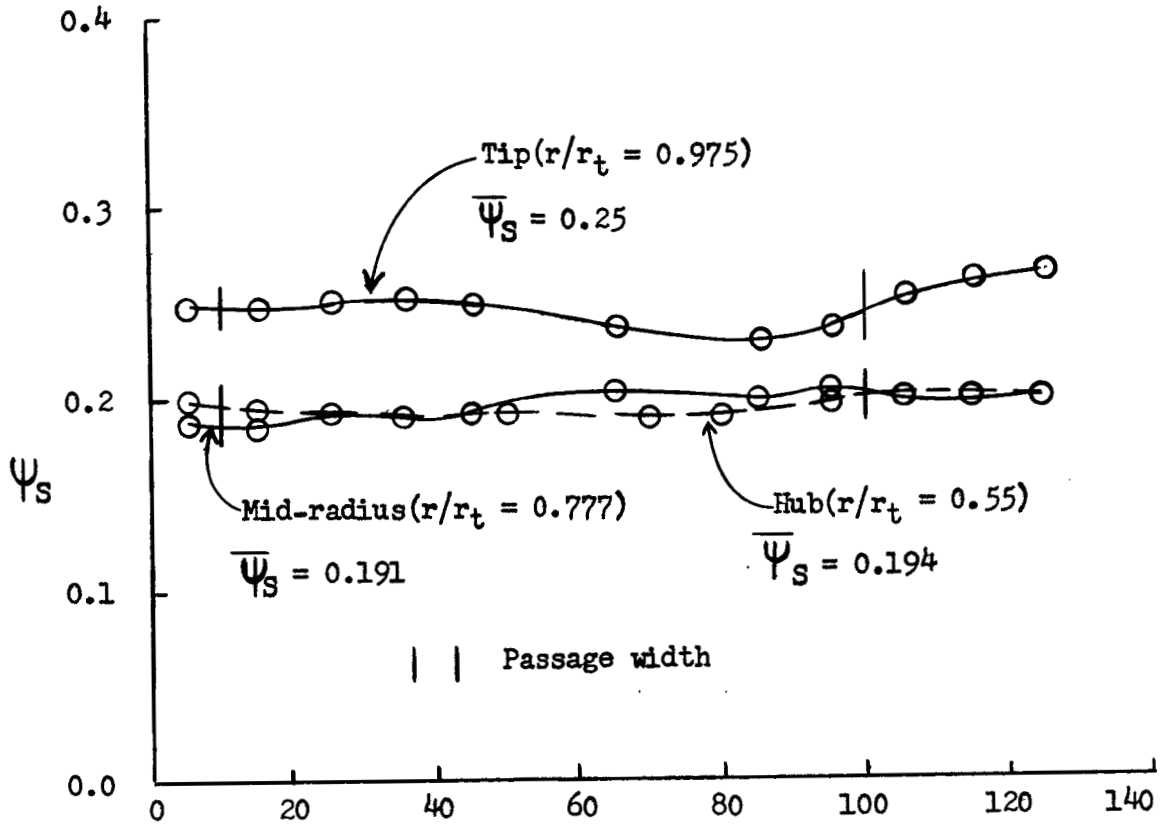

Figure 10: Circumferential Distribution of the Static Pressure Coefficient

Non-dimensional Total Pressure of the Absolute Flow

Radial location (r/r_t)	Spacial average derived from rotating probe measurements $\bar{\Psi}_{T_{ab}}$	Stationary probe measurements $\Psi_{T_{ab}}$	Per cent difference $\% = \frac{\Psi - \bar{\Psi}}{\bar{\Psi}}$
0.55	0.224	0.226	+.09%
0.777	0.270	0.321	+18.80%
0.975	0.448	0.527	+17.60%

Non-dimensional Static Pressure

Radial location (r/r_t)	Spacial average derived from rotating probe measurements $\bar{\Psi}_{T_{ab}}$	Stationary probe measurements $\Psi_{T_{ab}}$	Per cent difference $\% = \frac{\Psi - \bar{\Psi}}{\bar{\Psi}}$
0.55	.194	.206	+6.2%
0.777	.191	.233	+22.0%
0.975	.250	.291	+16.4%

Figure 11: Comparison of the Rotating and Stationary Pressure Probe Measurements

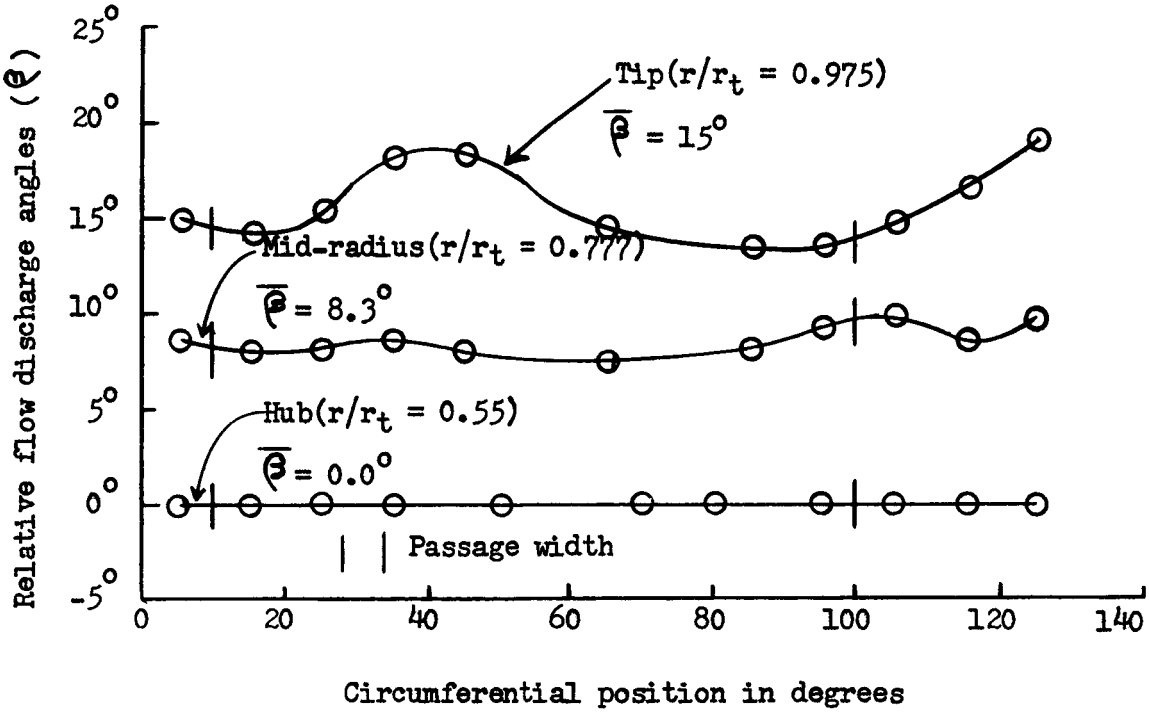

Figure 12: Circumferential Distribution of the Relative Flow Discharge Angles

		Tip(r/r_t = 0.975)							
		U/U_t	α	β	V/U_t	V_θ/U_t	V_x/U_t	W/U_t	W_θ/U_t
- - - - -	Design (From simplified radial equilibrium)	0.975	36.0°	5.3°	0.187	0.110	0.080	0.877	0.865
———	Based upon absolute flow measurements	0.975	25.0°	24.0°	0.528	0.478	0.223	0.545	0.497
— - —	Derived from spacial average relative flow measurements	0.975	19.5°	15.0°	0.446	0.421	0.148	0.574	0.554

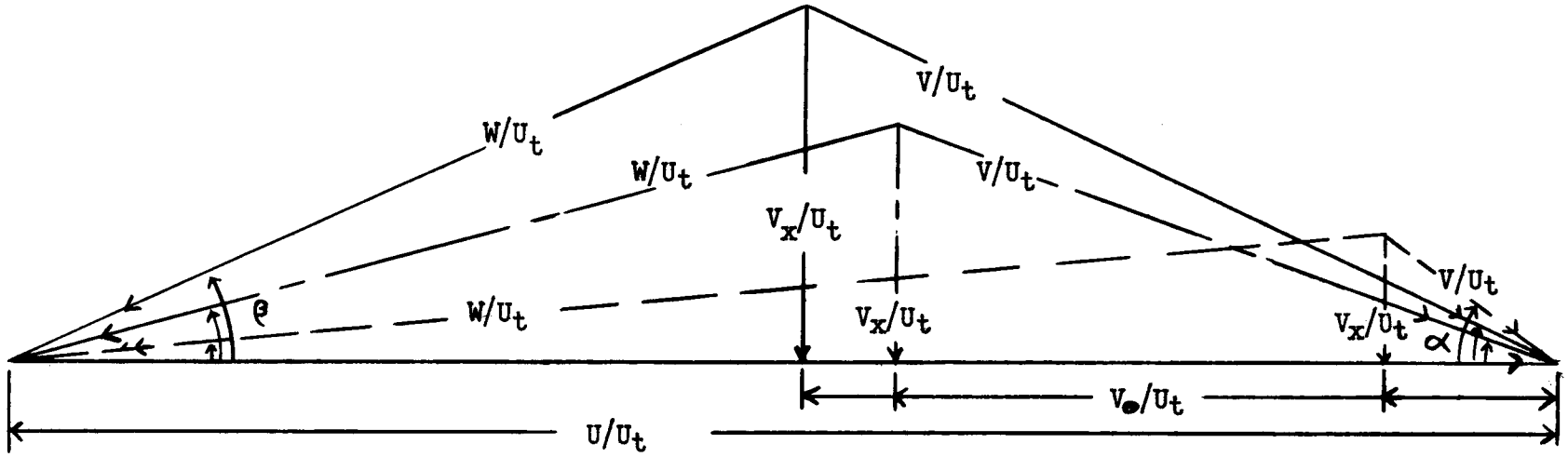

Figure 13(a): Comparison of the Design Velocity Triangles with the Velocity Triangles Derived from Relative and Absolute Flow Measurements

		Mid-radius(r/r_t = 0.777)							
		U/U_t	α	ε	V/U_t	V_θ/U_t	V_x/U_t	W/U_t	W_θ/U_t
- - - - -	Design (From simplified radial equilibrium)	0.777	25.4°	8.0°	0.198	0.179	0.085	0.607	0.598
———	Based upon absolute flow measurements	0.777	32.5°	19.6°	0.330	0.278	0.177	0.529	0.499
— - —	Derived from spacial average relative flow measurements	0.777	18.0°	8.3°	0.254	0.241	0.078	0.542	0.536

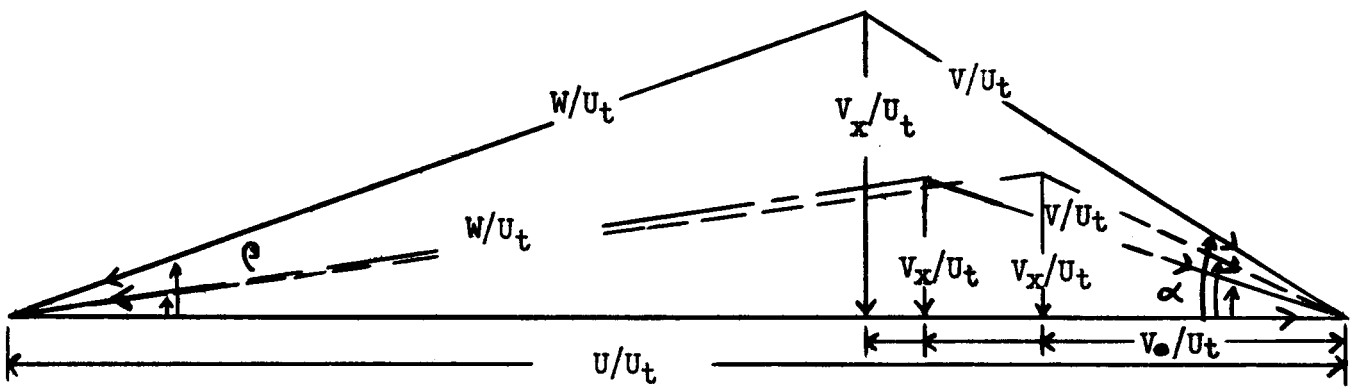

Figure 13(b): Comparison of the Design Velocity Triangles with the Velocity Triangles Derived from Relative and Absolute Flow Measurements

Hub($r/r_t = 0.55$)

		U/U_t	α	β	V/U_t	V_θ/U_t	V_x/U_t	W/U_t	W_θ/U_t
- - - - -	Design (From simplified radial equilibrium)	0.55	26°	17.4°	0.239	0.215	0.105	0.351	0.335
———	Based upon absolute flow measurements	0.55	0°	0°	0.161	0.161	0.0	0.389	0.389
— - —	Derived from spacial average relative flow measurements	0.55	0°	0°	0.170	0.170	0.0	0.380	0.380

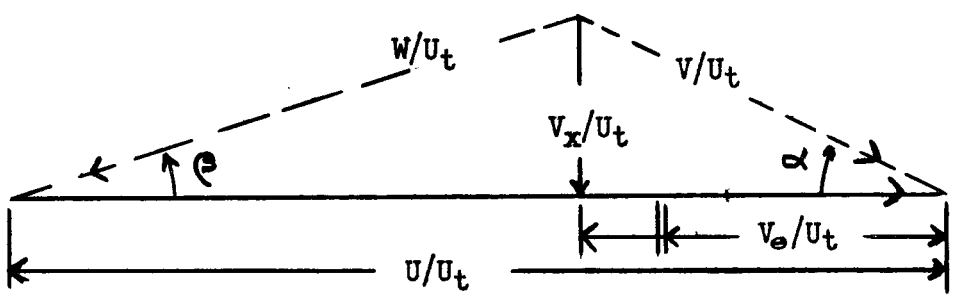

Figure 13(c): Comparison of the Design Velocity Triangles with the Velocity Triangles Derived from Relative and Absolute Flow Measurements

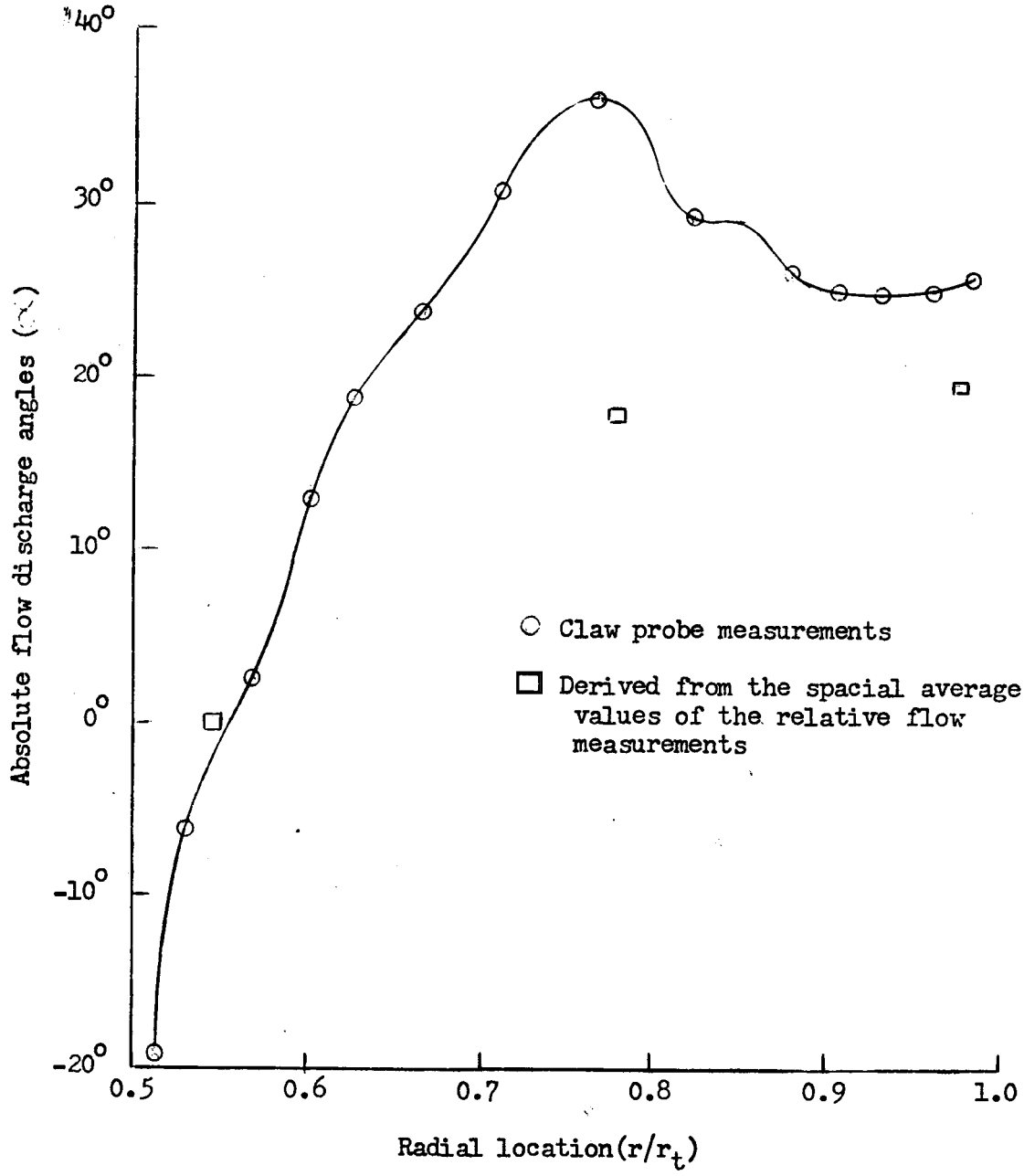

Figure 14: Comparison of the Absolute Discharge Flow Angles Derived from Relative Flow Measurements with Absolute Flow Claw Probe Measurements

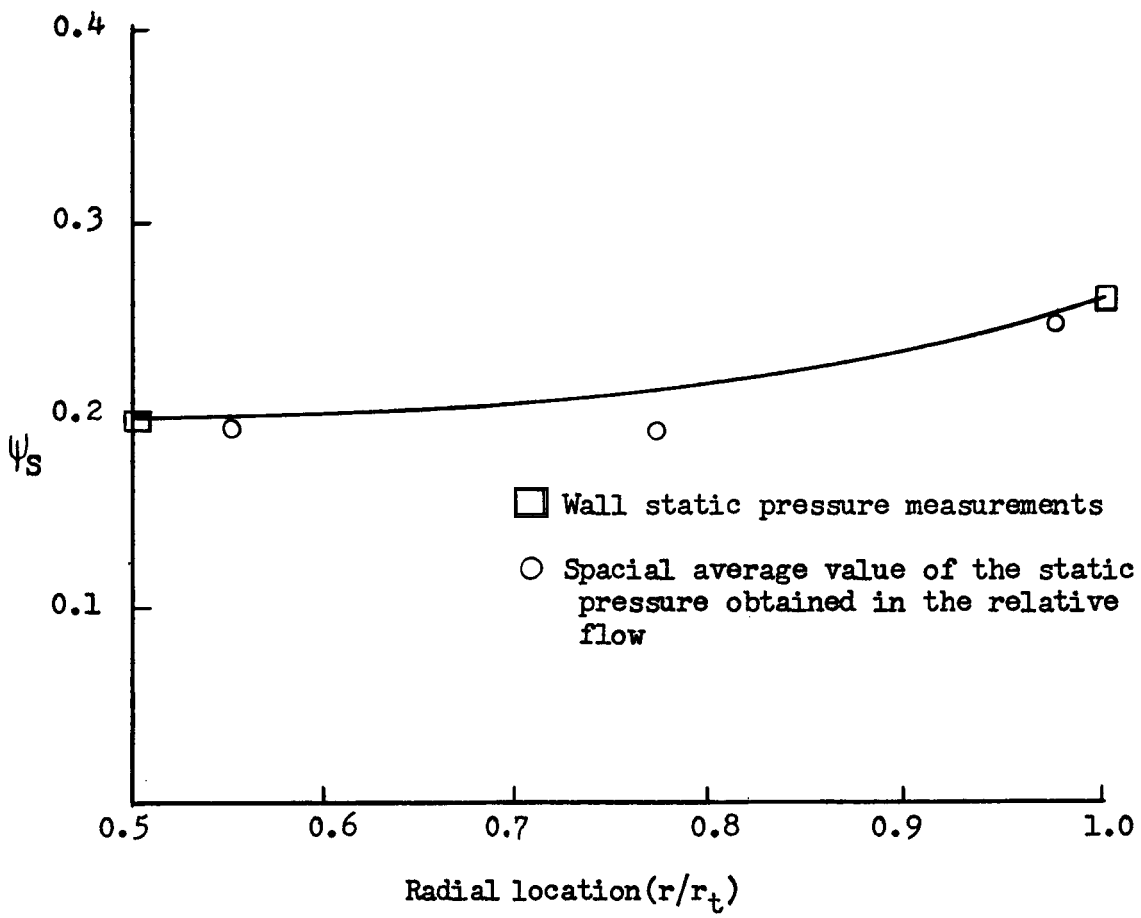

Figure 15: Comparison of the Measured Static Pressures with a Theoretical Curve Based upon Radial Equilibrium and Wall Static Pressure Measurements

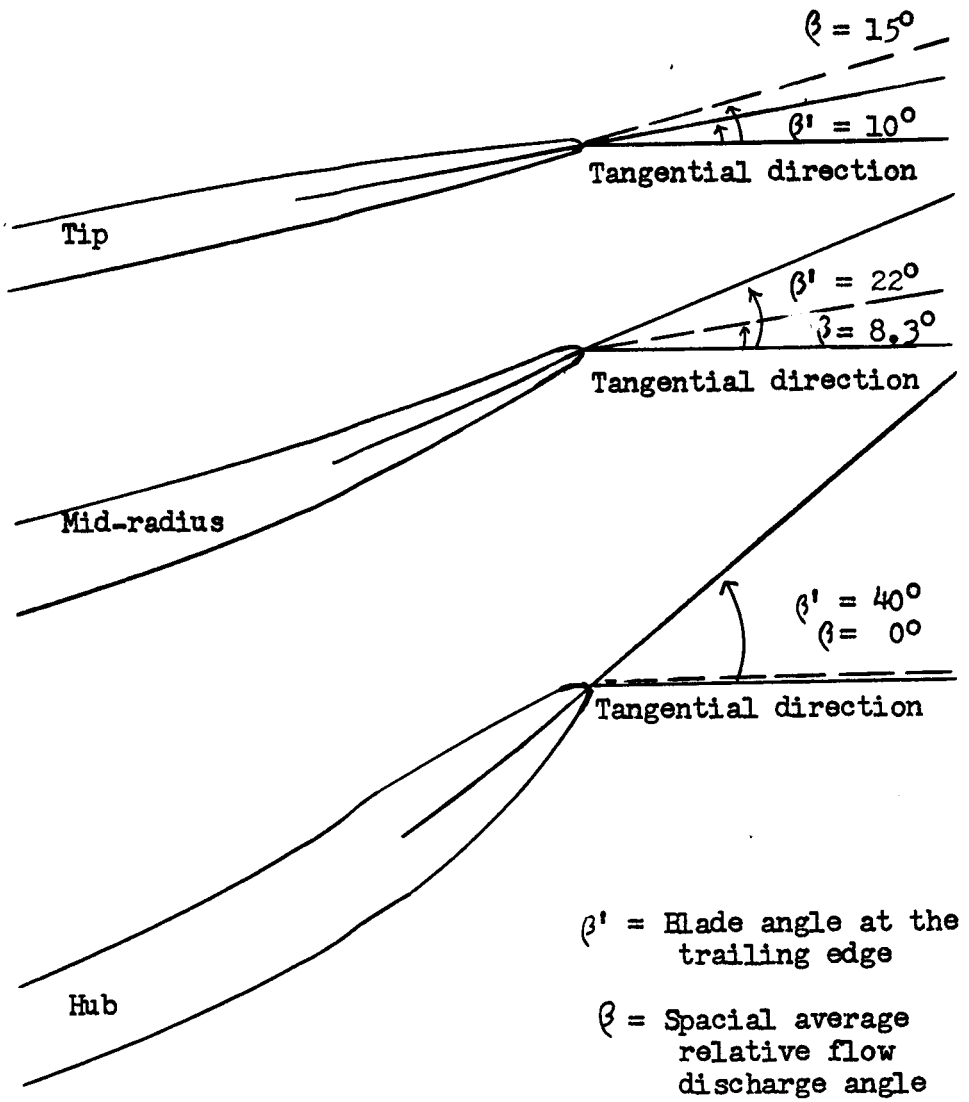

Figure 16: Comparison of the Spacial Average Discharge Relative Flow Angles with the Blade Angles at the Trailing Edge